Fluid interfacial nanoroughness measurement through the morphological characteristics of graphene

Hong Min Yoon,[1] Jung Shin Lee,[1] Jong-Souk Yeo,[2] and Joon Sang Lee[1,a)]
[1]*Department of Mechanical Engineering, Yonsei University, 50 Yonsei-ro, Seodaemun-gu, Seoul 120-749, South Korea*
[2]*School of Integrated Technology, Yonsei University, 162-1, Veritas Hall C, Songdo-dong, Yeonsu-gu, Incheon 406-840, South Korea*

(Received 28 June 2014; accepted 9 October 2014; published online 16 October 2014)

The interfacial nanoroughness of liquid plays an important role in the reliability of liquid lenses, capillary waves, and mass transfer in biological cells [Grilli *et al.*, Opt. Express **16**, 8084 (2008), Wang *et al.*, IEEE Photon. Technol. Lett. **18**, 2650 (2006), and T. Fukuma *et al.*, **92**, 3603 (2007)]. However, the nanoroughness of liquid is hard to visualize or measure due to the instability and dynamics of the liquid-gas interface. In this study, we blanket a liquid water surface with monolayer graphene to project the nanoroughness of the liquid surface. Monolayer graphene can project the surface roughness because of the extremely high flexibility attributed to its one atomic thickness. The interface of graphene and water is successfully mimicked by the molecular dynamics method. The nanoroughness of graphene and water is defined based on density distribution. The correlation among the roughness of graphene and water is developed within a certain temperature range (298–390 K). The results show that the roughness of water surface is successfully transferred to graphene surface. Surface tension is also calculated with a simple water slab. The rise of temperature increased the roughness and decreased the surface tension. Finally, the relationship between graphene roughness and surface tension is fitted with a second-order polynomial equation. © *2014 AIP Publishing LLC*.
[http://dx.doi.org/10.1063/1.4898756]

I. INTRODUCTION

The nanoroughness of the surface of a liquid has been widely investigated to understand the equilibrium thermodynamic property of surface tension, and it plays crucial role in a variety of applications.[1–3] Hence, experimental and theoretical methods have been developed to measure the nanoroughness of liquid surface. X-ray scattering and optical techniques are common experimental methods for observing the structure of a liquid surface. A variety of liquid surfaces, including argon, carbon tetrachloride, water, helium, alkanes, and alcohols, have been studied extensively (refer to Penfold's review).[4] Recently, Yang *et al.* used an atomic force microscope (AFM) to investigate the roughness of a liquid interface and successfully measured nanoroughness and its temperature dependency. This study implies that AFM can be used to measure the roughness of a highly flexible surface.[5] A theoretical approach, such as capillary wave (CW) theory, has also been used to study the structure of a liquid surface. Many researchers have validated their experimental results by comparing them with CW theory. Although CW theory interprets surface structures with surface wave-dependent parameters, a recent study found this theory to be valid up to the scale of a few molecules.[6] However, this approach has limitations when complex surface phenomena are considered, such as atomic-scale layering, molecular orientation preference, and surface freezing and melting, that can significantly affect the nanoroughness of the liquid surface.[4,7]

a)Electronic mail: joonlee@yonsei.ac.kr

Molecular dynamics (MD) simulation can provide an alternative solution to overcome these problems. Several studies have already proved the reliability of numerical methods for describing interfaces, including a liquid–vapor interface,[8–11] liquid–liquid interface,[12–14] and liquid–surfactant–liquid interfaces.[15,16] MD results show that an interface structure is strongly affected by molecular interaction; for example, the van der Waals parameter, ε, significantly affected the thickness of a water and oil interface.[13] Hydrogen bonding among molecules at an interface decides the orientation preference of molecules, which affects interfacial nanoroughness.[7] Differences in interfacial structure also affect the interfacial tension of the system.[16] Though many studies have been carried out, MD simulations have provided only fundamental information that is difficult to observe with current experimental techniques. Hence, research needs to be performed in order to develop the link between MD simulations and experiments and increase the applicability of the numerical approach.

In this study, we propose a new protocol to measure the nanoroughness of a liquid surface using the roughness of monolayer graphene floating on water. The out-of-plane motion of graphene is very sensitive to external conditions because of graphene's one atomic thickness. Furthermore, graphene roughness is more convenient to measure experimentally than a liquid surface. Several studies have revealed that graphene and water show strong morphological interactions.[17,18] Based on previous studies, we assume that the roughness of water's surface can be transferred to the surface of graphene floating on it.

Figure 1 describes the scheme of the present research. The correlation among two types of roughness (graphene floating on water, and a simple water surface) was studied using MD simulations. Information about the roughness was obtained from the density distributions. The surface tension of simple liquid water was calculated by the pressure distribution of a simple water system. Finally, we obtained the correlation equation between the nanoroughness of the graphene floating on the water surface and the surface tension of water.

II. SIMULATION METHODS

A. Simulation system

Figure 2 illustrates the simulation systems. MD simulations in the NPT ensemble were performed for two systems: type 1 and type 2. The system type 1 was composed by water and graphene, while the system type 2 consisted of only with water. The roughness of the graphene

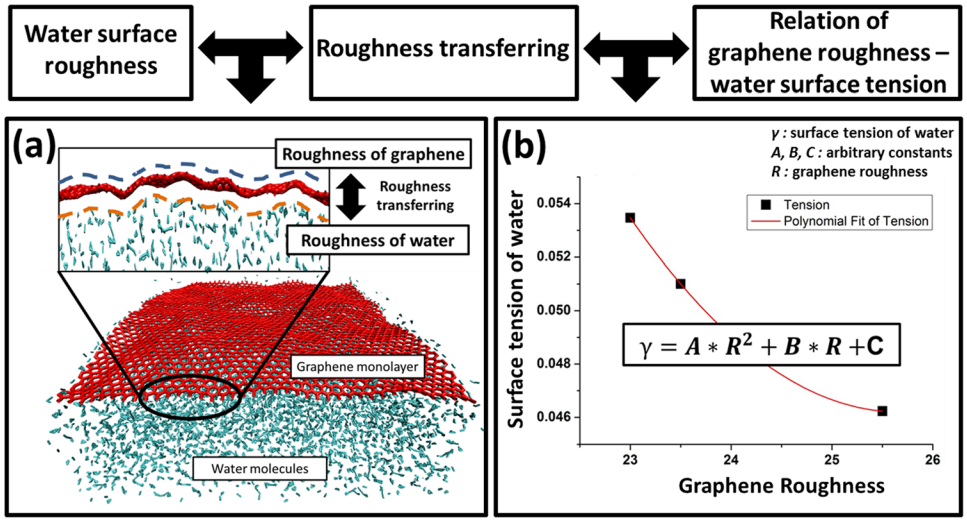

FIG. 1. A schematic diagram summarizing the objectives of the study. (a) Roughness of the liquid water surface is transferred to graphene monolayer. (b) After the roughness transferring process, the correlation equation of surface tension of water and graphene roughness is developed by the second order polynomial fitting.

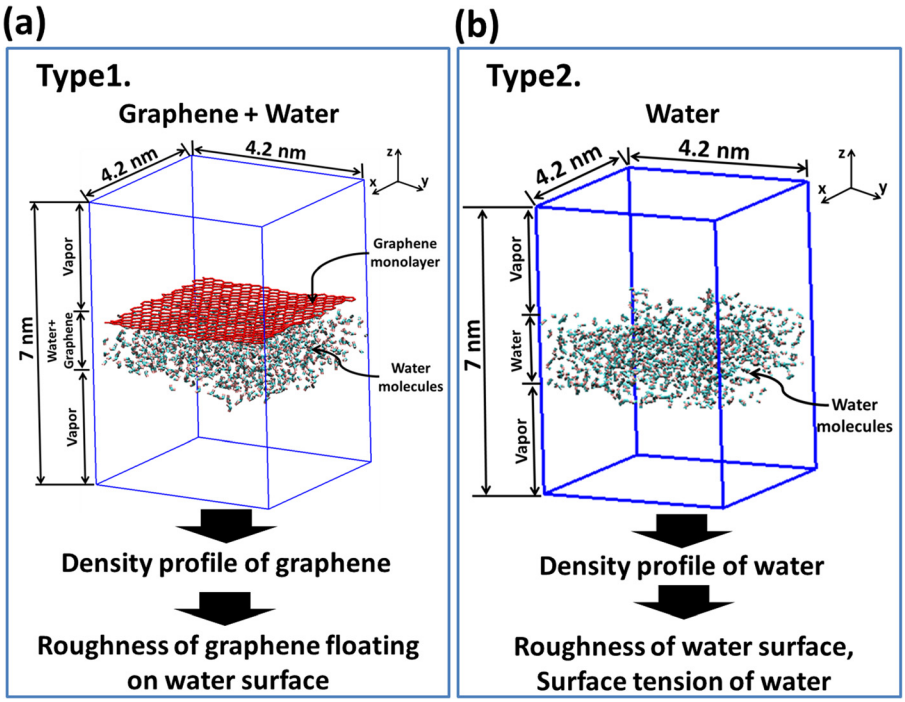

FIG. 2. Two types of simulation systems. (a) Type 1 is composed of liquid water, graphene and vapor phase. Type 1 simulations provide the roughness of the graphene floating on water. (b) Type 2 is composed of liquid water and vapor phase. Roughness and surface tension of water are calculated from type 2 simulations.

floating on water and simple water surface were calculated from type 1 and type 2, respectively. A periodic boundary condition was applied to the x, y, and z directions. The water slab and graphene contained 803 water molecules. We used a 4-nm × 4-nm graphene monolayer composed of 680 carbon atoms.

All carbon atoms were explicitly taken into account in all cases. Water molecule was modeled with the extended simple point charge (SPC/E) model. The water density at room temperature and the self-diffusion constant from SPC/E model are in good agreement with experimental result.[19] Lennard-Jones potential and Coulomb interaction were used to describe the interaction between water molecules. Lennard-Jones interaction between atoms, i and j, is defined as

$$V_{Lennard-Jones} = 4\epsilon\left[\left(\frac{\sigma}{r_{i,j}}\right)^{12} - \left(\frac{\sigma}{r_{i,j}}\right)^{6}\right], \tag{1}$$

where ϵ and σ are Lennard-Jones parameters and $r_{i,j}$ is the distance between the atoms, i and j, in the pairwise interaction. Coulomb potential is defined as

$$V_{Coloumb} = \frac{Cq_iq_j}{\epsilon r_{i,j}}, \tag{2}$$

where C represents Coulomb's constant. q_i and q_j are the signed magnitudes of the charges of atoms, i and j. Graphene monolayer was modeled with adaptive intermolecular reactive empirical bond order potential, which is widely used to mimic the structure and interfacial properties of graphene.[20–23] Water–carbon interactions were described with Lennard-Jones potential because graphene was mimicked as a neutral material. We followed the parameters used in the work of Gordillo and Martí for water–carbon interactions.[18] Translation and rotation of the center of graphene's mass were suppressed, and the z-position of the center of mass was fixed for

the water slab to inhibit the drift of the overall system. Fluctuating motion in the z-direction was only allowed to calculate the average roughness of graphene.

The vapor phases appeared at the top and bottom of the region in the simulation boxes, as shown in Fig. 2. Empty space was assumed to describe the vapor phase due to the density difference between liquid and vapor phases. Two vapor phases were located at both side of the simulation domain. This symmetric structure prevented the force unbalance and drifting of overall simulation system. Three simulation steps were carried out to construct stable vapor phases in type 1 and type 2. First, the z-length of the box was set to be 2 nm, and the initial system strain was removed by 100 ps of the microcanonical (NVT) ensemble. Then, the z-length of the box was expanded to 7 nm, with 200 ps in the second relaxation process with the isothermal-isobaric (NPT) ensemble. After all the relaxation procedures, 2 ns of additional simulations with NPT ensemble were performed to obtain the equilibrium properties such as roughness and surface tension.

The long-range Coulomb interactions among water molecules were calculated by the Ewald method.[24] The temperature of each case was controlled by a Nose-Hoover thermostat.[25,26] The temperature range from 298 to 390 K was chosen to minimize the effect of phase change. A 1 fs time-step was used for all cases. A large-scale atomic/molecular massively parallel simulator (LAMMPS) and Visual Molecular Dynamics (VMD) were used for calculations and post processing.

B. Pressure

All energy terms acting on atoms in the system were considered in the calculation of system pressure. The stress tensor of each atom was the sum of kinetic energy, pairwise interaction energy (which is 6–12 Lennard-Jones interactions), bond energy, and long-range Coulomb interactions. Overall system pressure was obtained by summing the stress tensor of all atoms. Stress tensor for atom i is defined as

$$S_{ab,i} = -\sum_{n=1}^{N}\left[m_i v_a v_b + \frac{1}{2}\sum_{\mathrm{n}=1}^{N_{pair}}(r_{ia}F_{ib} + r_{ja}F_{jb}) + \frac{1}{2}\sum_{n=1}^{N_{bond}}(r_{ia}F_{ib} + r_{ja}F_{jb}) + \frac{1}{3}\sum_{n=1}^{N_{angle}}(r_{ia}F_{ib} + r_{ja}F_{jb} + r_{ka}F_{kb}) + Ksapce(r_{ia}, F_{ib})\right], \quad (3)$$

where a and b are the direction of the tensor component. Also, i, j, and k represent atomic index. N is a number of each contribution. Stress tensor consists of five components. The first term is a kinetic energy of atom i. m_i represents mass of atom i, and v_a and v_b are the velocities for corresponding direction. The second term is short range pairwise interaction contribution. r_{ia} and r_{ja} are the position of two atoms in the pairwise interaction. F_{ib} and F_{jb} are the forces on atoms i and j resulting from short range pairwise interaction. The third term is covalent bond energy contribution. The fourth term is angle energy contribution. The last term is long range pairwise interaction and Coulomb interaction contributions. Long range forces were calculated in K-space. Ewald summation method was applied for all calculations.

C. Surface tension

To calculate surface tension, two interfaces of water–vapor were assumed to be perpendicular to the z-axis. We used the following Kirkwood-Buff equation:[27]

$$\gamma = -\frac{1}{2}\left(\frac{P_{xx} + P_{yy}}{2} - P_{zz}\right)L_z, \quad (4)$$

where P_{xx}, P_{yy}, and P_{zz} represents a pressure component in x, y, and z direction, respectively. L_Z represents the box length in the z-direction.

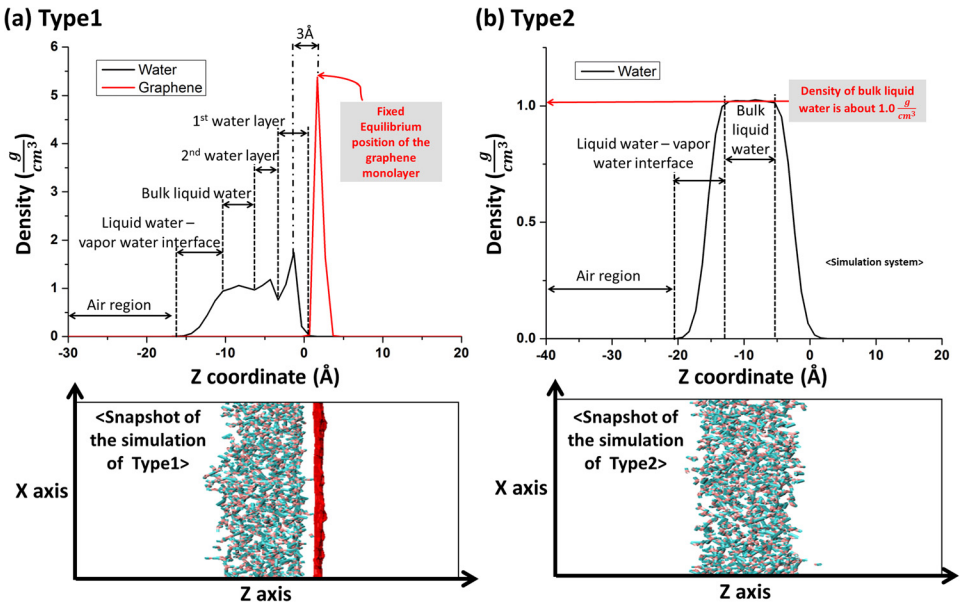

FIG. 3. Density distributions and snapshots of (a) type 1 (water-graphene system) and (b) type 2 (water system). Both the density profiles clearly show the existence of interface and bulk liquid phase of water.

III. RESULTS

A. Density distributions

In Fig. 3, the density distributions of type 1 and type 2 simulations are plotted. The temperature in both cases was 298 K. The distributions of all components, including water and graphene, were calculated along with the z axis. Our data were averaged over 2 ns. The snapshots of both type 1 and type 2 system represent the corresponding geometries which were observed in our simulation.

In Fig. 3(a), the graphene monolayer plotted in red line shows a peak-shaped distribution. The initial z-position of the carbon atoms in the graphene was set to be zero, and overall drift of the graphene monolayer was suppressed. Hence, the width of the peak implies that graphene fluctuated along the z direction. In Fig. 3(a), the black solid line clearly shows the layered structure of the water molecules. Each peak in the distribution of water represents a layer of water molecules. These layers were formed by the effect of the graphene monolayer. Peak shape is distinct up to the second layer, and the distance between the peaks of first water layer and graphene is about 3 Å. These results are in agreement with Gordillo and Martí's results.[18] The rest of the distribution represents the bulk liquid water and the liquid water–vapor interface. In the MD simulation, the vapor phase can be modeled as empty space because vapor density is much lower than that of liquid.

In Fig. 3(b), the density distribution of water molecules in type 2 is shown. We constructed two symmetrical interfaces to minimize the force imbalance of the overall system. The plot is divided into three regions: bulk liquid water, liquid water–vapor interface, and vapor. The density plot stays constant in the bulk liquid water region. The density is about $1\frac{g}{cm^3}$, which corresponds to the literature.[28] Density starts to drop at the end of the bulk liquid water region. This trend of decrease continues until the water density reaches zero. We defined these regions as interfaces, referring to the concept of Gibbs surface excess. In the vapor region, the density of water is almost zero.

B. Definitions of graphene roughness and interface

The graphene roughness and the interface of liquid water–vapor should be defined mathematically to obtain the correlation equation. Figure 4 describes the definition of graphene roughness and the interfacial region based on the density distributions.

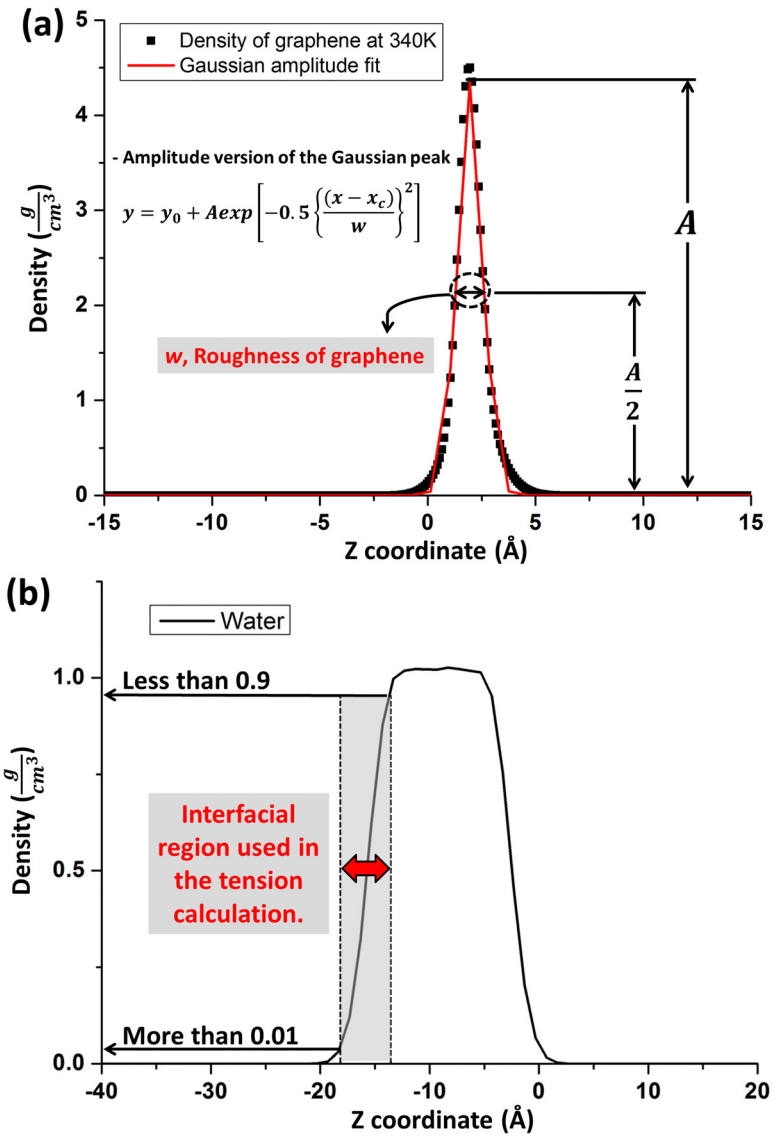

FIG. 4. Definitions of the roughness of graphene and water. (a) Graphene roughness is defined as full width at half maximum value of amplitude version of the Gaussian peak. (b) Roughness and interfacial region of water are defined by the water density of $0.01 \sim 0.9\ \frac{g}{cm^3}$.

In Fig. 4(a), the black squares represent the simulation results. We fitted the results using the amplitude version of the Gaussian peak function, which is plotted as the red line. The formula of the fitting function is written in Fig. 4(a). In the formula, the term w is used as the graphene roughness, which is the full width at half the maximum of the fitting curve.

In Fig. 4(b), the grey region indicated by the filled red arrow represents the liquid water–vapor interface. We modified the so-called "10–90" width method.[29,30] Equilibrium liquid water and vapor density were assumed to be $1\ \frac{g}{cm^3}$ and $0\ \frac{g}{cm^3}$, respectively. In the interfacial region, the water density was within $0.01 \sim 0.9\ \frac{g}{cm^3}$. This range of density was chosen to remove the effect of large pressure fluctuations from the water–vapor region, which will be discussed in Sec. III D.

C. Relation of the roughness of graphene and water

The surface of water at 390 K is represented as the isosurface image in Fig. 5. All atoms were assumed to have spherical shape. The snapshot clearly shows the rough surface morphology of the water surface at the interface.

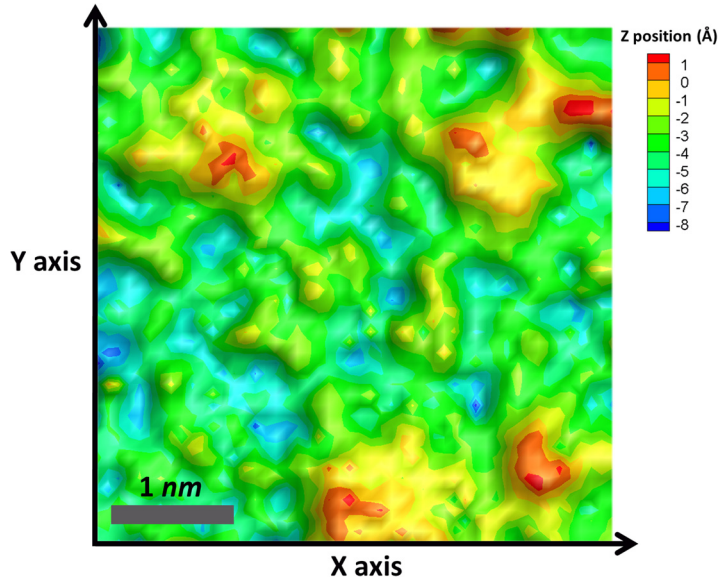

FIG. 5. Isosurface snapshot of the water surface of type 2 simulation at 390 K.

Figure 6 shows the temperature dependency of the roughness of graphene in type 1 and water in type 2. The definitions of roughness were defined in Sec. III B. Filled black squares and filled blue circles represent the variation of the roughness of graphene in type 1 and that of water in type 2, respectively. Empty blue triangles and empty blue diamonds represent the roughness of water surface from the references. The magnitude of the roughness of water surface in type2 is in agreement with Matsumoto and Kataoka's results,[31] as shown in Fig. 6. Our result is larger than Taylor's results due to the larger interfacial area which is related with the capillary wave.[9]

Roughness of graphene and water increases as temperature increases. In Fig. 6, the variation magnitudes of the roughness of graphene and water surface are 0.04 Å and 4 Å, respectively. The result shows that the magnitude of roughness of water is scaled down to the order of 10^2 when it is transferred to graphene surface. The scaled down roughness came from the strong covalent bonding in graphene compared to the weak non-covalent bonding among water

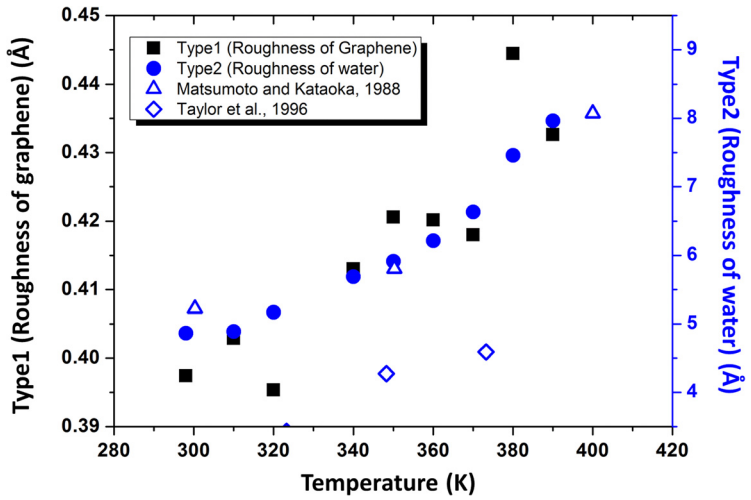

FIG. 6. Temperature dependency of the roughness of graphene in type 1 and water surface in type 2. Empty blue triangles and empty blue diamonds each represent the roughness of water in the previous studies. Increasing trends of the roughness of graphene (filled black squares) and water (filled blue circles) are similar.

molecules. The trend of the variation is similar. Thus, the roughness of water surface can be indirectly calculated by measuring the roughness of graphene floating on water. This implies that graphene can be used to transfer the roughness of water surface.

D. Pressure distribution

In Eq. (2), surface tension is defined as a pressure difference in lateral and vertical direction. The definition of surface tension indicates that the pressure distribution can be used to describe the characteristics of the water-vapor interface. In Fig. 7, pressure distribution is plotted along the z-direction. The pressure of the type 2 simulation was calculated by summing the stresses of all atoms, as defined in Eq. (1). Black squares, red circles, and blue triangles represent P_{xx}, P_{yy}, and P_{zz}, respectively. The pressure distribution clearly shows the characteristics of the interface. The plot can be divided into four regions: bulk liquid water, liquid water–vapor water interface, vapor water–air interface, and bulk air. The pressure distribution in bulk phase is isotropic.

However, pressure is anisotropic at the interface. P_{xx} and P_{yy} represent the lateral pressure whose direction is parallel to the interface. P_{zz} is the vertical pressure whose direction is perpendicular to the interface. The vertical pressure is much larger than the lateral pressure at the liquid water–vapor interface. In Eq. (1), pressure includes terms of pairwise and Coulomb interactions. Each water molecule is fully surrounded by other water molecules in the lateral direction, whereas each was only half surrounded in the vertical direction. This situation causes force imbalance. A water molecule at the interface is strongly attracted to the bulk phase by pairwise interactions. This induces the high positive value of vertical pressure. The pressure difference between lateral and vertical directions is calculated as surface tension.

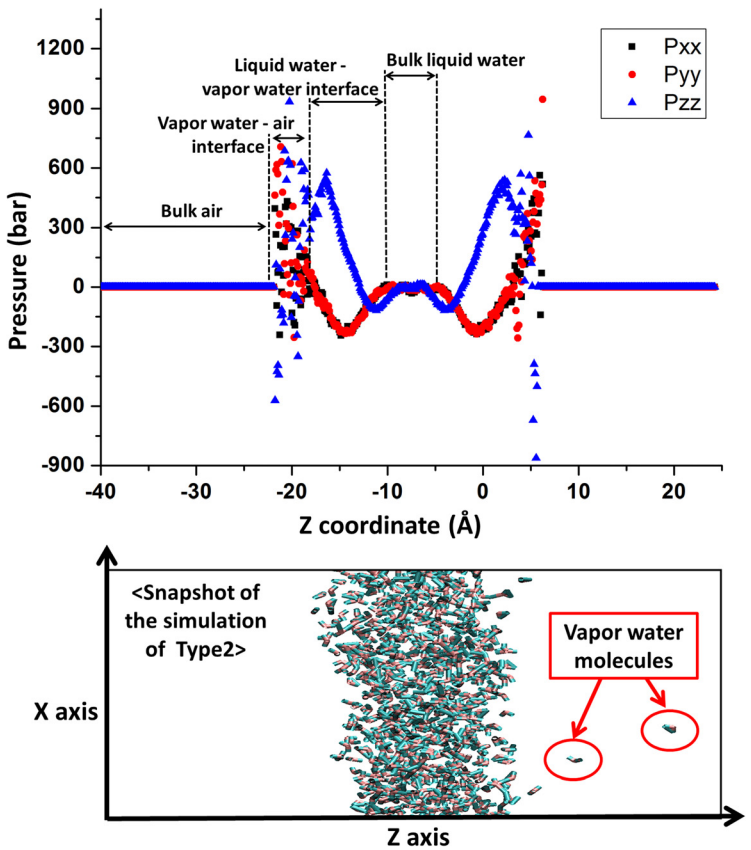

FIG. 7. Pressure distribution and snapshot of the type 2 simulation. Pressure distribution shows the structure of liquid water and air interface. Snapshot describes vapor water molecules that were escaping from the liquid water phase.

The vapor water–air interface developed between bulk air and the liquid water–vapor interface. All pressure components fluctuated significantly in this region. The large fluctuations primarily come from the high kinetic energy of water molecules. During the simulations, several molecules escaped from the liquid water slab. In Fig. 7, the snapshot clearly show vapor water molecules. These molecules traversed the vapor region with an extremely high velocity compared to molecules in the liquid regions. This trend clearly increased as the system temperature increased.

E. Correlation of roughness and surface tension

We varied temperature to obtain the correlation equation of the surface tension and graphene roughness. Surface tension and graphene roughness were normalized by dividing the

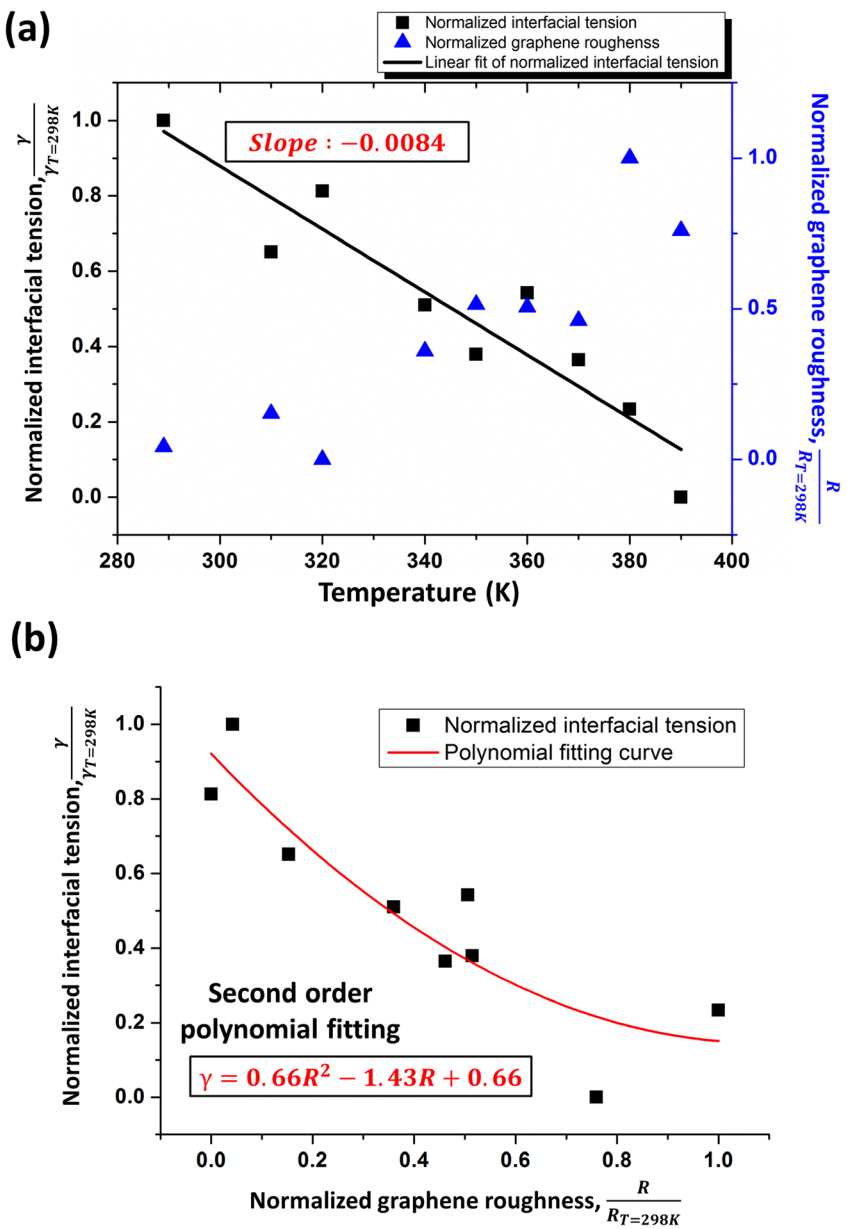

FIG. 8. (a) Temperature dependency of the normalized surface tension and graphene roughness. Normalized surface tension has the decreasing trend with the slope of −0.0084, which is in agreement with the result of Shi *et al.*[32] (b) The correlation equation of surface tension and graphene roughness. Second order polynomial equation is fitted with simulation results.

results by 298 K. In Fig. 8(a), the plot clearly shows that the normalized surface tension decreases as the temperature increases. The slope of the linear fit curve is −0.0084, which is similar to the results of Shi *et al*.[32] In Fig. 8(b), we formulated the correlation equation of the normalized surface tension and graphene roughness based on the result in Fig. 8(a). The plot shows that normalized surface tension decreases as normalized graphene roughness increases. In CW theory, surface tension is proportional to the inverse of the square of roughness.[6] Our result is well fitted by a second-order polynomial equation, which provides a direct relation between the roughness of graphene floating on the water surface and the surface tension of the water.

IV. CONCLUSIONS

We simulated the interface between graphene and water to determine the roughness relationship between graphene and water. The roughness of graphene floating on water surface has not been studied directly by both experiment and simulation. Hence, the results were validated indirectly in each section. Graphene-water (type 1) and water (type 2) systems were successfully modeled by MD simulations. The density distributions of type 1 showed that water developed a layer structure under graphene. The monolayer graphene clearly affected up to the second water layer which well agrees with the other studies. In type 2, the pressure distribution had proven the existence of bulk liquid water, liquid water–vapor water interface, water vapor water–air interface, and bulk air regions. The high positive pressure in the vertical direction at the interface was due to the half-surrounded condition of water molecules, which had caused the imbalance of force. Roughness of water surface was calculated by modifying "10–90" width method. Roughness of both cases increased with the rise of temperature. The magnitude of the roughness of water surface well matched with the other studies. The relation between roughness of water and graphene showed that the magnitude of roughness of water is scaled down to the order of 10^2, and the trend of the variation is similar. This result implied that the roughness of water surface was successfully transferred to graphene surface. Surface tension was also calculated with the difference between lateral and vertical pressure. The rise in temperature decreased the surface tension. Based on the simulation results, the relation of graphene roughness and surface tension was fitted with a second-order polynomial equation. Roughness of graphene can be easily measured by experimental technique, such as atomic force microscopy. However, further study is needed to examine the effect of system size on the roughness transferring procedure, which is crucial issue to develop the link between MD simulations and experiments.

ACKNOWLEDGMENTS

This work was supported by a grant from the Mid-career Researcher Program of the National Research Foundation of Korea (NRF) funded by the Ministry of Science, ICT, & Future Planning (Grant No. NRF-2013R1A2A2A01015333).

[1]S. Grilli, L. Miccio, V. Vespini, A. Finizio, S. D. Nicola, and P. Ferraro, Opt. Express **16**, 8084 (2008).
[2]J. J. Wang, A. Nikolov, and Q. Wu, IEEE Photon. Technol. Lett. **18**, 2650 (2006).
[3]T. Fukuma, M. J. Higgins, and S. P. Jarvis, Biophys. J. **92**, 3603 (2007).
[4]J. Penfold, Rep. Prog. Phys. **64**, 777 (2001).
[5]C. Y. Yang, F. H. Ho, P. J. Wang, and J. A. Yeh, Langmuir **26**, 6314 (2010).
[6]R. Delgado-Buscalioni, E. Chacón, and P. Tarazona, J. Phys. Condens. Matter **20**, 494229 (2008).
[7]G. Hantal, P. Terleczky, G. Horvai, L. Nyulászi, and P. Jedlovszky, J. Phys. Chem. C **113**, 19263 (2009).
[8]R. M. Townsend and S. A. Rice, J. Chem. Phys. **94**, 2207 (1991).
[9]R. S. Taylor, L. X. Dang, and B. C. Garrett, J. Phys. Chem. **100**, 11720 (1996).
[10]S. W. Sides, G. S. Grest, and M. Lacasse, Phys. Rev. E **60**, 6708 (1999).
[11]T. Chang, K. A. Peterson, and L. X. Dang, J. Chem. Phys. **103**, 7502 (1995).
[12]T. Chang and L. X. Dang, J. Chem. Phys. **104**, 6772 (1996).
[13]A. R. van Buuren, S. J. Marrink, and H. J. C. Berendsen, J. Phys. Chem. **97**, 9206 (1993).
[14]N. Sieffert and G. Wipff, J. Phys. Chem. B **110**, 13076 (2006).
[15]K. Esselink, P. A. J. Hilbers, N. M. van Os, B. Smit, and S. Karaborni, Colloids Surf., A **91**, 155 (1994).
[16]A. R. van Buuren and H. J. C. Berendsen, Langmuir **10**, 1703 (1994).
[17]A. Chialvo, L. Vlcek, and P. T. Cummings, J. Phys. Chem. C **117**, 23875 (2013).

[18]M. C. Gordillo and J. Martí, Phys. Rev. B **78**, 075432 (2008).
[19]H. J. C. Berendsen, J. R. Grigera, and T. P. Straatsma, J. Phys. Chem. **91**, 6269 (1987).
[20]S. J. Stuart, A. B. Tutein, and J. A. Harrison, J. Chem. Phys. **112**, 6472 (2000).
[21]K. Min and N. R. Aluru, Appl. Phys. Lett. **98**, 013113 (2011).
[22]Z. Xu and M. J. Buehler, ACS Nano **4**, 3869 (2010).
[23]H. M. Yoon, S. Kondaraju, and J. S. Lee, Tribol. Int. **70**, 170 (2014).
[24]D. M. Heyes, Phys. Rev. B **49**, 755 (1994).
[25]S. Nosé, J. Chem. Phys. **81**, 511 (1984).
[26]W. G. Hoover, Phys. Rev. A **31**, 1695 (1985).
[27]J. G. Kirkwood and F. P. Buff, J. Chem. Phys. **17**, 338 (1949).
[28]R. C. Weast, M. J. Astle, and W. H. Beyer, *CRC Handbook of Chemistry and Physics*, 69th ed. (CRC Press, Inc., Boca Raton, 1988).
[29]G. A. Chapela, G. Saville, S. M. Thomson, and J. S. Rowlinson, J. Chem. Soc., Faraday Trans. 2 **73**(7), 1133 (1977).
[30]B. Q. Lu, R. Evans, and M. M. Telo da Gama, Mol. Phys. **55**, 1319 (1985).
[31]M. Matsumoto and Y. Kataoka, J. Chem. Phys. **88**, 3233 (1988).
[32]B. Shi, S. Sinha, and V. K. Dhir, J. Chem. Phys. **124**, 204715 (2006).